

## RESEARCH REPORT

# A vertebrate-specific and essential role for *osterix* in osteogenesis revealed by gene knockout in the teleost medaka

Tingsheng Yu<sup>1,2,\*</sup>, Martin Graf<sup>1,2,\*</sup>, Joerg Renn<sup>1,2,†</sup>, Manfred Schartl<sup>3,4</sup>, Daria Larionova<sup>5</sup>, Ann Huysseune<sup>5</sup>, Paul Eckhard Witten<sup>5</sup> and Christoph Winkler<sup>1,2,§</sup>

## ABSTRACT

*osterix* (*osx*; *sp7*) encodes a zinc-finger transcription factor that controls osteoblast differentiation in mammals. Although identified in all vertebrate lineages, its role in non-mammalian bone formation remains elusive. Here, we show that an *osx* mutation in medaka results in severe bone defects and larval lethality. Pre-osteoblasts fail to differentiate leading to severe intramembranous and perichondral ossification defects. The notochord sheath mineralizes normally, supporting the idea of an osteoblast-independent mechanism for teleost vertebral centra formation. This study establishes a key role for *Osx* for bone formation in a non-mammalian species, and reveals conserved and non-conserved features in vertebrate bone formation.

**KEY WORDS:** Osteoblasts, Osteogenesis, Bone modelling, Skeleton, Medaka

## INTRODUCTION

Osteoblasts are bone matrix-forming cells that differentiate from *Sox9*- and *Runx2*-positive mesenchymal progenitors, which also give rise to chondrocytes and adipocytes (reviewed by Akiyama et al., 2005; Harada and Rodan, 2003; Ytteborg et al., 2015). The zinc-finger domain transcription factor *Osx* (also known as *Sp7*) is expressed in cells of the osteoblast lineage as well as in pre-hypertrophic chondrocytes, and is essential for embryonic and postnatal osteoblast differentiation in mice (Baek et al., 2010; Nakashima et al., 2002; Zhou et al., 2010). Severe bone defects caused by absence of osteoblasts, concomitant with ectopic cartilage formation, were reported in *Osx* null mice, suggesting that *Osx* is implicated in skeletal cell fate decisions (Koga et al., 2005; Nakashima et al., 2002). Importantly, a single base pair deletion in the *OSX* gene of a human patient with osteogenesis imperfecta has also been reported (Lapunzina et al., 2010). Therefore, a key regulatory role for *Osx* in mammalian bone formation is well-established, and many downstream targets and interactors have been identified (Hojo et al., 2016; Long, 2012).

However, whether a similarly important role for bone formation is conserved also in non-mammalian vertebrates, including teleost fish, remains unknown. Two recent reports described the generation of *osx* mutants in members of the cyprinid family, the common carp (*Cyprinus carpio*) and zebrafish (*Danio rerio*) (Kague et al., 2016; Zhong et al., 2016). Interestingly, these mutants are viable and exhibit recognizable bone defects only at later stages of life. In contrast to observations in mouse, bone formation during embryonic and juvenile development was not blocked, raising doubts of a highly conserved role of *osx* during vertebrate osteogenesis. This suggested a delay in osteoblast maturation rather than a crucial function for *osx* in these cyprinid mutants.

Medaka is a teleost fish with intramembranous and perichondral formation of bone that, in contrast to mammals and zebrafish, lacks osteocytes (for an overview, see Witten and Huysseune, 2009). Medaka and zebrafish *osx* orthologues are expressed in pre-mature and mature osteoblasts, as in mice (DeLaurier et al., 2010; Renn and Winkler, 2009; Spoorendonk et al., 2008). In the present study, we generated medaka *osx* mutants and observed severe bone defects caused by defective bone matrix deposition and early lethality of mutant juveniles.

## RESULTS AND DISCUSSION

*Osx* in vertebrates

To trace the evolutionary origin and phylogenetic distribution of *osx*, we searched chordate genomes for homologues of medaka *osx* (Fig. 1A; see supplementary Materials and Methods for details). No such gene was found in the available genomes of tunicates, cephalochordates and lampreys. A clear orthologue of *osx* is present in the genomes of the elephant shark and the coelacanth. *osx* is also present in all teleosts and in spotted gar. Within tetrapods, we found homologues in amphibians, reptiles and mammals. A peculiar situation exists in birds. Although in most of the 71 available high quality avian genomes no trace of an *osx* homologue was found, in seven species an *osx*-like gene is present. Despite full conservation of the *osx* diagnostic DNA-binding domain (Hojo et al., 2016), higher divergence in the rest of the protein made inclusion of these genes in a phylogenetic tree inappropriate. Presence or absence of this gene does not follow any phylogenetic pattern. For confirmation, a conserved synteny analysis was done. *osx* was always found within a cluster of orthologous genes and tightly linked to its paralogue *sp1* (Fig. S1). In bird species for which synteny information of the *sp1* region is available, and in which we found an *osx*-like gene, it resides exactly at the expected position. In all other birds, there is no other gene or even traces of a gene from the Sp transcription factor family besides *sp1*. Extant jawless vertebrates (hagfish and lampreys) represent a group that never had a mineralized dermal skeleton (Janvier, 2015). It thus appears that *osx* emerged by a local genome duplication at the base of either the ‘ostracoderms’ (an informal term referring to jawless vertebrates

<sup>1</sup>Department of Biological Sciences, National University of Singapore, Singapore 117543, Singapore. <sup>2</sup>Centre for Bioimaging Sciences (CBIS), National University of Singapore, Singapore 117543, Singapore. <sup>3</sup>Department of Physiological Chemistry, Biocenter, University of Würzburg, and Comprehensive Cancer Center Mainfranken, University Clinic Würzburg, Würzburg 97080, Germany. <sup>4</sup>Texas Institute for Advanced Study and Department of Biology, Texas A&M University, College Station, TX 77843, USA. <sup>5</sup>Department of Biology, Research Group Evolutionary Developmental Biology, Ghent University, Ghent B-9000, Belgium. \*Present address: A\*STAR, Institute of Molecular and Cell Biology (IMCB), Proteos, Biopolis, 61 Biopolis Drive, Singapore 138673. †Present address: Laboratory for Organogenesis and Regeneration, GIGA, University of Liege, Liege 4000, Belgium.

§Author for correspondence (dbswcw@nus.edu.sg)

© C.W., 0000-0002-0330-6692

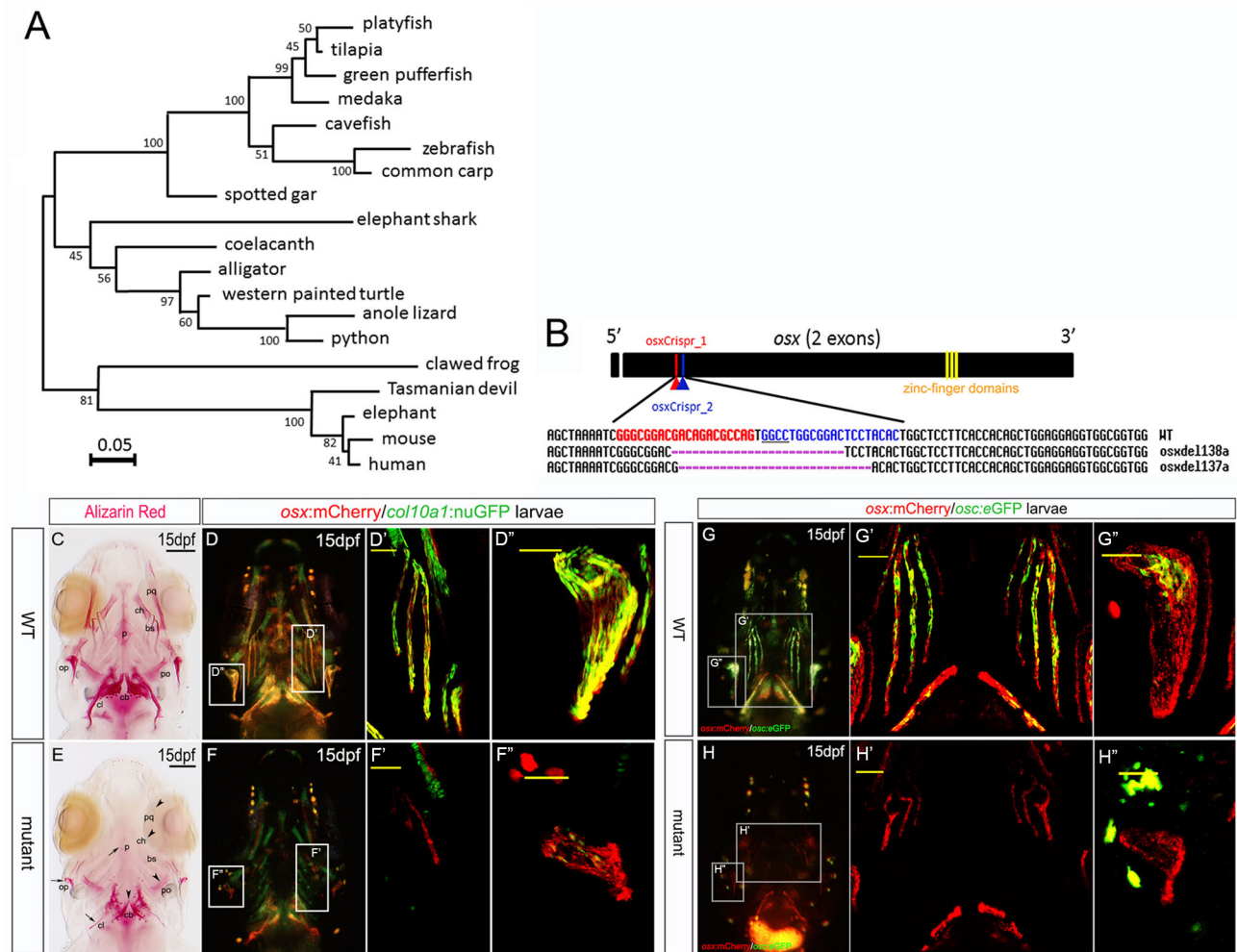


**Fig. 1. Phylogenetic distribution of *osx* and severe intramembranous bone defects and arrested osteoblast differentiation in medaka *osx* mutants.** (A) Relationship of *Osx* protein sequences among gnathostome groups. Numbers above branches are bootstrap values from a total of 1000 replicates. Note that several deep nodes are not highly supported due to the high similarity of vertebrate *Osx* (Sp7) proteins. (B) *osx* *Crispr\_1* (red) and *osx* *Crispr\_2* (blue) target sites in exon 2 of *osx*. The *HaeIII* site used for genotyping is underlined. Alignment of wild-type *osx* with *osx<sup>del138a</sup>* and *osx<sup>del137a</sup>* is shown below. (C,E) Alizarin Red-stained bone matrix in the cranium of a wild-type (C) and *osx* mutant (E) at 15 dpf. Intramembranous bones are missing, such as parasphenoid (p) and branchiostegal rays (bs), or severely reduced, such as operculum (op) and cleithrum (cl) (arrows). Also, perichondral bones are absent or severely reduced, as seen in the palatoquadrate (pq), ceratohyal (ch), paired prootics (po) and fifth ceratobranchial (cb) (arrowheads). (D-D'',F-F''). Distribution of *col10a1:nuGFP*- and *osx:mCherry*-expressing premature osteoblasts in wild-type (D) and *osx* mutant (F) medaka, ventral views. Boxed areas in D and F are shown at higher magnification in D' and F' (branchiostegal rays) and in D'' and F'' (operculum). Note areas in D' and D'' where *col10a1:nuGFP* and *osx:mCherry* expression is mutually exclusive, but most pre-osteoblasts co-express both markers. Note also the absence of *col10a1:nuGFP* and reduced numbers of *osx:mCherry* cells in *osx* mutants. (G-H'') *osx:mCherry*- and *osc:eGFP*-positive osteoblasts in wild-type (G-G'') and *osx* mutant (H-H''). Boxed areas are shown at higher magnification in G' and H' (branchiostegal rays) and in G'' and H'' (operculum). Note the presence of fully differentiated, *osx:mCherry*- and *osc:eGFP*-expressing osteoblasts in the operculum centre and branchiostegal rays in wild type but absence of *osc:eGFP*- and reduction of *osx:mCherry*-expressing cells in *osx* mutant. Scale bars: 150  $\mu$ m (B,D); 50  $\mu$ m (D-D'',F-F'',G-H'').

with a dermal skeleton) or the jawed vertebrates (gnathostomes). *osx* was obviously lost repeatedly in the avian lineage and retained only in a handful of species. Further investigations are needed to explain how this loss could have occurred without disrupting bone formation.

### CRISPR/Cas9-induced mutations in *osx* prevent bone but not cartilage formation in medaka

*osx* *Crispr\_1* and *Crispr\_2* guide RNAs (gRNAs) were co-injected with Cas9 mRNA into *osx:mCherry* transgenic medaka embryos (Fig. 1B). The number and distribution of *osx*-positive osteoblasts were affected in the vertebral bodies of injected larvae (Fig. S2) suggesting osteoblast differentiation defects in this transient CRISPR (clustered regularly interspaced short palindromic

repeats) assay. Only 23 out of 138 injected embryos developed into adulthood. Ten out of 23 did not show obvious skeletal or other malformations, and five of those were genotyped as mutant from fin clips (Fig. S2A). These were used for generation of F1 embryos. Different types of insertion-deletion (indel) mutations were detected in heterozygous F2 adult fish. Two alleles (*osx<sup>del138a</sup>*, 25 bp deletion; *osx<sup>del137a</sup>*, 28 bp deletion) result in frameshifts and premature stop codons at amino acid positions 138 and 137, respectively, upstream of the three zinc-finger DNA-binding domains (Fig. 1B). We performed qPCR analysis in *osx* mutants and found a 70% reduction in *osx* transcript levels (Fig. S3). We cannot exclude the possibility that the remaining transcripts contribute to residual *Osx* activity. However, this is unlikely given the positions of the introduced mutations, which are deduced

to result in a truncated protein lacking the essential zinc-finger domain. Homozygous carriers for both alleles were obtained and showed identical phenotypes (Fig. S4). Therefore, only *osx*<sup>del137a</sup> mutant phenotypes are described below.

Alizarin Red staining revealed reduction or absence of intramembranous bone formation in *osx* mutants, i.e. the operculum, parasphenoid and branchiostegal rays (Fig. 1C,E). Ultrastructural analysis showed reduced bone matrix formation in branchiostegal rays and cleithrum (Fig. S5). The number and patterning of teeth appeared normal in mutants, although tooth sizes were generally smaller in mutants compared with wild-type siblings (Fig. S6A,B). Detailed observations revealed that the smaller tooth size in mutants was due to less dentin being deposited and to the absence of attachment bone that normally connects the tooth to the underlying bone (Fig. S6C,D). Although the evolutionary history of attachment bone remains unresolved, this phenotype might be in line with a role for *Osx* in root, but not crown, dentin formation in mice (Zhang et al., 2015). The notochord sheath-based vertebral centra anlagen of *osx* mutants appeared to be normally mineralized (Fig. S7A,B). By contrast, the neural arches of vertebral bodies were completely lacking. No bone matrix and no Alizarin Red staining was detected (Fig. S7C,D).

Less than 1% of *osx* mutants ( $n > 100$  mutants analysed) survived beyond one month of age, and none beyond two months. Mutant one-month-old fish lacked scales and showed an almost complete absence of neural and hemal arches, as well as ribs, and lacked bony fin rays of all paired and unpaired fins (Fig. S8). They were also small in size and lacked most of the mineralized cranial skeleton. Thus, in this respect, medaka *osx* mutants recapitulate bone formation and mineralization defects reported in mouse mutants (Nakashima et al., 2002), confirming that *osx* is a crucial player in bone formation in non-mammalian vertebrates. However, unlike in the mouse model (Oh et al., 2012), the formation of cartilage appeared to be normal in medaka *osx* mutants (Fig. S9). Although the ectopic cartilage observed in mouse *osx* mutants (Oh et al., 2012) could be a consequence of delayed *Osx*-controlled perichondral ossification, we suggest that *osx* is dispensable for chondrocyte maturation in medaka.

### Medaka *osx* mutants fail to undergo osteoblast differentiation during intramembranous and perichondral ossification

Next, transgenic osteoblast reporter expression was analysed in wild-type and *osx* mutant larvae. Expression in the *osx*:mCherry reporter line closely follows the endogenous *osx* transcription pattern but is slightly delayed due to maturation of newly translated reporter protein (Renn and Winkler, 2009). Transgenic and endogenous *osx* expressions precede the onset of bone mineralization and continue in mature osteoblasts (Renn and Winkler, 2009). Expression of *osteocalcin* (*osc*) and the transgenic *osc*:eGFP reporter is found only in mature osteoblasts during ongoing ossification (Inohaya et al., 2007; Renn and Winkler, 2009). Also, *collagen10a1* (*col10a1*) reporter expression in bone cells follows the endogenous expression pattern. However, *col10a1*:nuGFP reporter expression is also found in cartilage, where endogenous *col10a1* expression cannot be detected at the corresponding stages, suggesting possible position defects at the transgene insertion site (Renn et al., 2013). Live imaging of *osx*:mCherry- and *col10a1*:nuGFP-labelled cells in the cranium of *osx* mutants (Fig. 1D,F) revealed an almost complete absence of *col10a1*-positive pre-osteoblasts in intramembranous bones such as the branchiostegal rays (Fig. 1F') and operculum (Fig. 1F'').

Interestingly, although the number of *osx*:mCherry-positive cells was reduced in these bones, some cells persisted, which suggested that a limited number of pre-osteoblasts can form. These cells exhibit *osx* promoter activity but are unable to switch on other pre-osteoblast markers such as *col10a1*. Ultimately, these *osx*-deficient cells fail to differentiate into mature functional osteoblasts and are not able to produce collagen-containing osteoid. This was confirmed by analysing matured osteoblasts, which express *osteocalcin* (*osc*) (Inohaya et al., 2007). *osc*:eGFP-positive cells were completely missing in the operculum and branchiostegal rays of *osx* mutant fish (Fig. 1G,H). Over-exposure with 24-fold higher laser power revealed that only few cells with very low *osc*:eGFP expression remained in the cleithrum

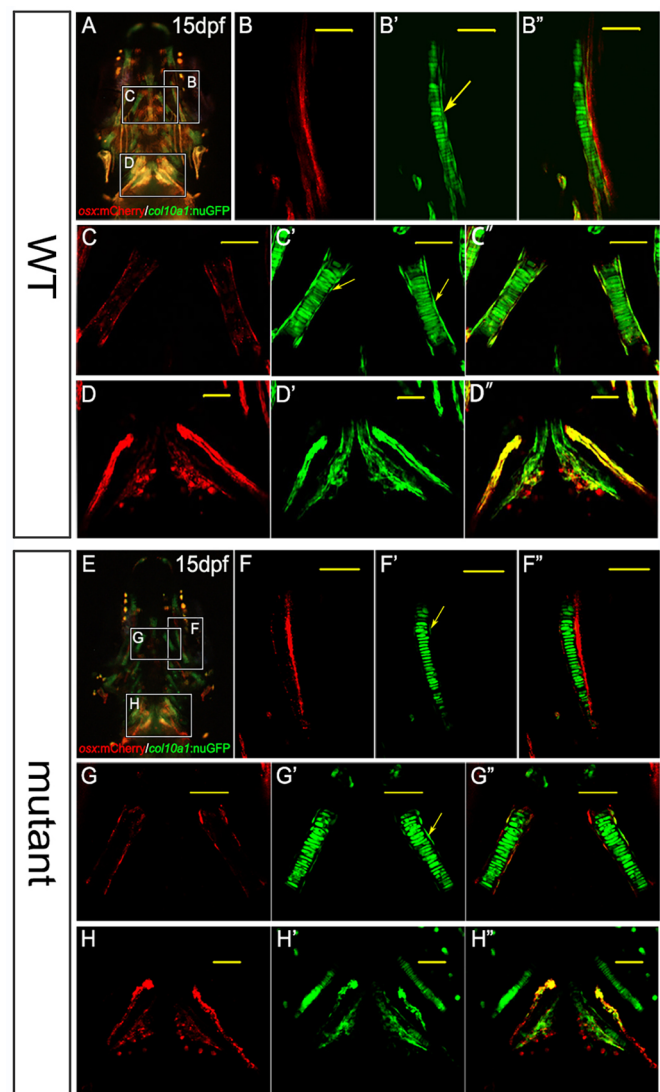


**Fig. 2. Reduced numbers of perichondral osteoblasts in medaka *osx* mutants.** (A–D') Analysis of chondrocytes and *col10a1*:nuGFP/*osx*:mCherry double-positive perichondral osteoblasts (arrows in B' and C') in wild-type medaka. Boxed areas in A are shown as confocal images at higher magnification in B–B' (palatoquadrate), C–C' (ceratohyal) and D–D' (ceratobranchials 5). (E–H') In *osx* mutants, *col10a1*:nuGFP-expressing perichondral osteoblasts are almost absent in the palatoquadrate (arrow in F') and only residual cells are seen in the ceratohyal (arrow in G'). Note that strong mCherry expression in the palatoquadrate might be due to mCherry aggregation of non-functional cells (F). Expression in teeth and cartilage of the fifth ceratobranchials is similar to wild type (H–H'). Scale bars: 50  $\mu$ m.



(Fig. S10), validating the conclusion that osteoblast maturation was generally blocked in *osx* mutants. This shows that *osx* is required for differentiation of most osteoblasts in medaka, with the exception of a few cells that start to differentiate into osteoblasts independently of *osx*, possibly due to an unknown compensatory mechanism.

Perichondral osteogenesis, i.e. bone formation on a previously established cartilage scaffold, was also affected in *osx* mutants. *col10a1:nuGFP/osx:mCherry* double-positive pre-osteoblasts were absent from the palatoquadrate (Fig. 2B',F'). Interestingly, a few of these perichondral cells remained in the mutant ceratohyal (Fig. 2C-C'',G-G''), and these cells only expressed *col10a1:nuGFP* and not *osx:mCherry*. This might reflect a possible chondrocytic origin of these particular perichondral cells as proposed by Hammond and Schulte-Merker (2009) for zebrafish. These cells probably fail to fully differentiate into osteoblasts in the absence of *osx* function. Chondrocytes positive for *col10a1:nuGFP* appeared to form normally (Fig. 2B',F'), consistent with our observation that cartilage matrix formation is normal in medaka *osx* mutants (Figs S4,S9).

### Osteoblast progenitor specification is affected in *osx* mutants

As osteoblast differentiation was blocked in *osx* mutants, we next analysed whether osteoblast progenitor cells form normally. RNA *in situ* hybridization at 4 and 6 days post-fertilization (dpf) revealed that transcription of *runx2*, a general marker for osteoblast and chondrocyte progenitor formation (Flores et al., 2004; Li et al., 2009), was strongly reduced (Fig. 3A–D). By contrast, transcription of the chondrocyte marker *col2a* was normal, as expected (Fig. 3E,F). Comparable with our findings using the *osx:mCherry* reporter line, transcription of *osx* was slightly reduced especially in the parasphenoid and operculum (Fig. 3G,H), and it remains to be determined whether this reduction is due to nonsense-mediated decay of the mutant mRNA. Interestingly, *col10a1* (Fig. 3I,J) and *osc* (Fig. 3K,L) transcripts were almost completely absent. This shows that not only is differentiation of *osx* cells into mature *osc*-expressing osteoblasts blocked in medaka *osx* mutants but the formation of *runx2*-positive osteoblast progenitors and *col10a1*-expressing pre-osteoblasts is also affected. These findings suggest that medaka *osx*

has a so far unknown role in osteoblast progenitor specification. Alternatively, it is possible that formation of osteoblast progenitors depends on the presence of mature osteoblasts and/or mineralized bone. This is strikingly different from the situation in *Osx* null mice, in which *Runx2* expression was not affected (Nakashima et al., 2002), but similar to the situation in zebrafish *osx* mutants at 6 weeks post-fertilization (Kague et al., 2016).

### *osx* is required for perichordal bone formation but not notochord sheath mineralization

Besides ossification defects in the cranium, we also observed deficiencies in the developing vertebral column. Mineralized arches and their bone matrix were absent in *osx* mutants. By contrast, vertebral centra anlagen, which in teleost fish form by mineralization of the notochord sheath (Huxley, 1859; K  lliker, 1859), were present and regularly mineralized (Fig. 4A,F). Vertebral centra and arches constitute developmental modules (Lauder, 1980; Hautier et al., 2010). Recent studies did indeed confirm the independent development (modularity) of vertebral centra and arches. For example, in the *stocksteif* (*dol*, *cyp26b1*) mutant zebrafish and in malformed Atlantic salmon, vertebral centra fuse whereas arches remain separated (Witten et al., 2006; Laue et al., 2008; Spoorendonk et al., 2008). By contrast, zebrafish *fused somites* (*fss*, *tbx6*) mutants have fused arches but retain separated vertebral centra (van Eeden et al., 1996). Modularity of vertebral centra and arches is also displayed during normal development of teleosts, such as in the caudal fin endoskeleton of zebrafish (Bensimon-Brito et al., 2012a).

Live imaging showed that *osx:mCherry*- and *osc:eGFP*-positive cells were strongly reduced in number in both arches and centra (Fig. 4B,D,G,I). By contrast, the number of *col10a1:nuGFP*-positive cells was normal in the mutant vertebral centra (Fig. 4C,E,H,J). This supports the idea that *col10a1:nuGFP*-positive but *osx:mCherry*-negative cells regulate mineralization of the notochord sheath in medaka as suggested earlier (Renn et al., 2013). The strong similarities in composition between notochord sheath and cartilage matrix, and the fact that *col10a1* expression is a prerequisite for cartilage mineralization (Kirsch and von der Mark, 1992) can further explain a requirement of *col10a1:nuGFP*-positive cells for

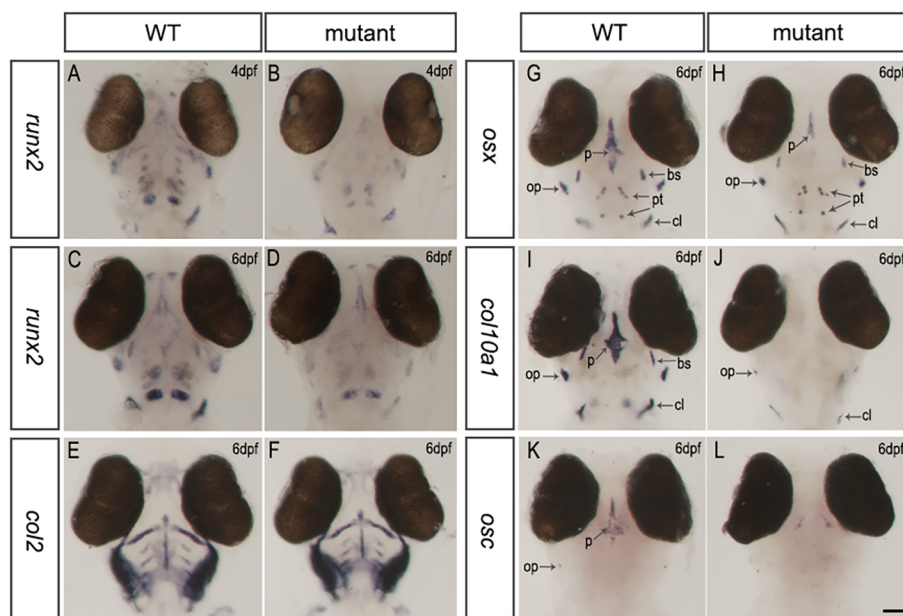


**Fig. 3. Pre-osteoblast markers are downregulated in medaka *osx* mutants.**

(A–D) RNA *in situ* hybridization showing reduced transcription of *runx2* in mutants at 4 and 6 dpf (B,D) compared with wild type (WT; A,C). (E,F) Normal transcription of *col2* in both WT and mutants. (G,H) Slightly reduced *osx* transcription in *osx* mutants (H) compared with WT (G). (I–L) Almost complete absence of *col10a1* (J) and *osc* (L) transcripts in mutants compared with WT (I,K). bs, branchiostegal rays; cl, cleithrum; op, operculum; p, parasphenoid; pt, pharyngeal teeth. Scale bars: 50 µm.

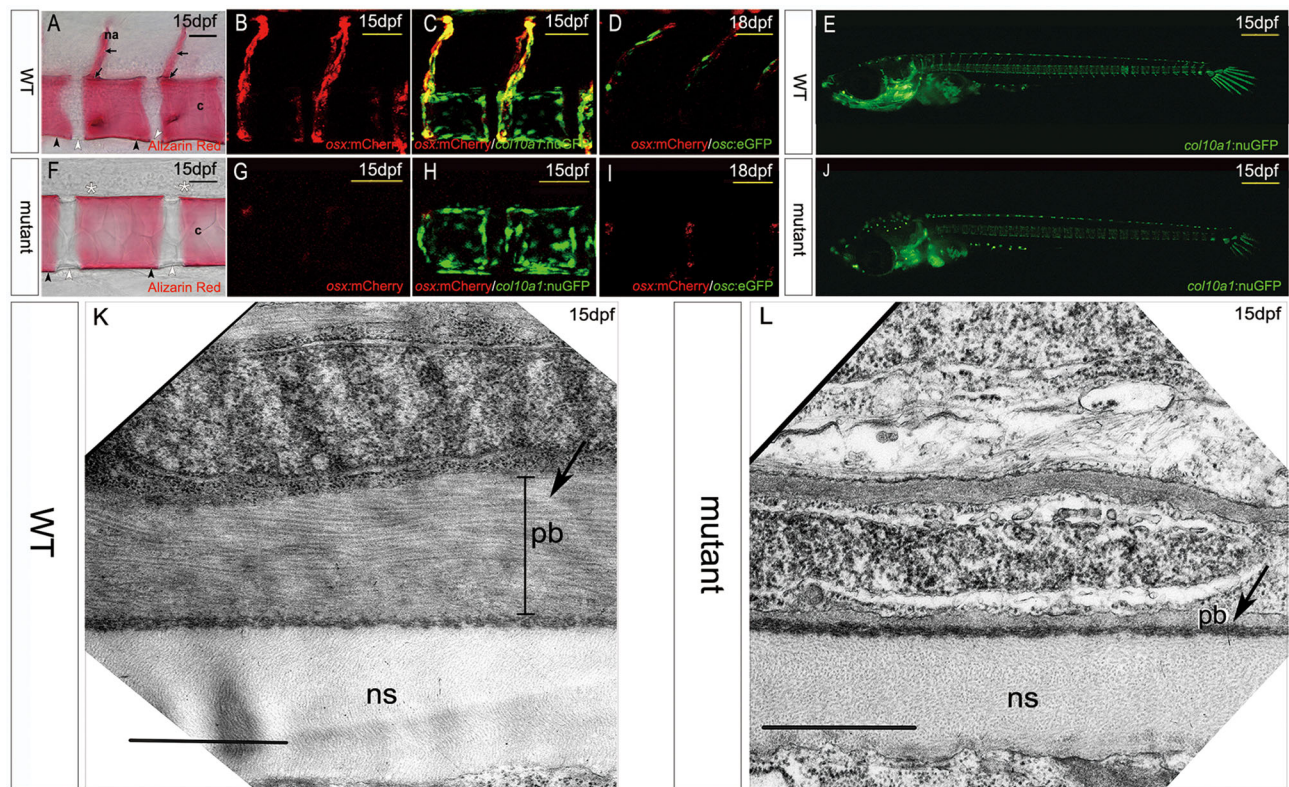


**Fig. 4. Normal mineralization of notochord sheath, but absence of perichordal bone in the centra of medaka *osx* mutants.** (A) Alizarin Red-stained wild-type (WT) vertebral body showing the non-mineralized notochord sheath of the intervertebral space (white arrowheads), the mineralized notochord sheath of the vertebral centrum (black arrowheads) and the bone of the neural arch and bone at the basis of the neural arch (black arrows). (B–D) Confocal images of wild-type fish at 15 dpf (B,C) and 18 dpf (D) showing normal distribution of osteoblasts along the mineralized neural arches (na) and centra (c) (as indicated in A). Lateral views. (E) Lateral view of *col10a1:nuGFP* transgenic medaka larva. (F) Alizarin Red-stained mutant vertebral body, labelled as in A. White asterisks indicate positions of missing neural arches. (G–I) Confocal images of vertebral bodies in *osx* mutants. Centra lack mineralized neural arches and show decreased numbers of *osx:mCherry* (G), *col10a1:nuGFP* (H) and *osc:eGFP* (I) cells in the arch region. *col10a1:nuGFP* cells are abundant in centra of mutants (H). (J) *col10a1:nuGFP* expression in *osx* mutant. (K,L) Transmission electron microscopy images showing normal thickness of the notochord sheath (ns) but almost complete absence of perichordal bone matrix (pb). Scale bars: 40  $\mu$ m (A,F); 50  $\mu$ m (B–D,G–I); 300  $\mu$ m (E,J); 1  $\mu$ m (K,L).

notochord sheath mineralization. Future experiments analysing the activity of alkaline phosphatase in *col10a1:nuGFP* cells are needed to confirm the capacity of these cells to facilitate centra mineralization, similar to what has been shown for the notochord epithelium in salmon and zebrafish (Bensimon-Brito et al., 2012b; Grotmol et al., 2005).

Transmission electron microscopy revealed normal thickness of the notochord sheath (ns) in *osx* mutants and the almost complete absence of bone matrix outside the notochord (perichordal bone, pb) (Fig. 4K,L, black arrows), supporting the idea that *osx*-positive osteoblasts are not required for notochord sheath formation or for cartilage formation but are essential for bone matrix formation (Fleming et al., 2015).

In striking difference to recent reports on *osx* mutants in carp and zebrafish (Kague et al., 2016; Zhong et al., 2016), we observed strong defects in embryonic and larval bone formation after *osx* knockout in medaka, leading to early adult lethality in homozygous mutants and vertebral malformations in heterozygous carriers (Fig. S11). Generally, the bone defects in mutants appeared to be more severe than those that we previously reported in morphants after *osx* knockdown (Renn and Winkler, 2014). For example, *col10a1* and *osc* expression was almost completely absent in the parasphenoid of mutants, whereas residual expression remained in morphants. The progenitor marker *runx2* was strongly reduced in *osx* mutants but appeared normal in morphants (Fig. 3; compare with figure 4 in Renn

and Winkler, 2014). Whereas bone defects, such as in the vertebral arches, eventually recovered in morphants, they persisted in mutants resulting in early lethality. Together, the mutant data provide evidence for an essential role of *osx* in osteoblast differentiation in medaka that was not completely evident in morphants.

Findings that *osx*-deficient carp and zebrafish show relatively normal initial bone patterning and formation could suggest that *osx* is dispensable for bone formation in these species. Given the role of *osx* in mammalian bone formation and given that it is required for bone formation in medaka, this explanation appears, however, unlikely. There are several possibilities to explain the incomplete phenotype of the *osx* mutants in carp and zebrafish. The carp has a tetraploid genome (Xu et al., 2014) and harbours two copies of *sp7*, both of which function in bone formation (Zhong et al., 2016). In such situations, the still-intact second copy can be expected to take over, at least partially, the function of the mutant copy. The *sp7* gene of zebrafish has a peculiar genomic structure with a gain of two additional introns. The premature stop codon mutation lies in the small exon 2. A compensatory alternative splice event could skip this exon and create shorter transcripts that would code for a protein that still contains the majority of the wild-type protein, most importantly the DNA-binding zinc fingers. On a more general level, it is possible that other *osx*-related Sp genes, such as *sp1*, have a compensatory role in osteogenesis in zebrafish and carp. Sp7 and Sp1 – but also Sp3, and possibly other Sp factors – can bind to the same promoters, as has



been shown in osteoblastic cells (Goto et al., 2006). Convincing evidence has also been presented that as-yet-unknown compensatory networks that involve genes unrelated to the one carrying the mutation become activated once a key developmental regulator is compromised (Rossi et al., 2015). It is conceivable that compensatory mechanisms are lineage specific and are in place in the two cyprinids (zebrafish and carp) but absent in medaka.

Still, our study highlights possible differences in aspects of *osx* function between mammals and teleosts. In medaka, either directly or indirectly, *osx* appears to control osteoblast progenitor specification, which has not been reported for mice. Despite these differences, our results demonstrate a significant degree of functional conservation between teleosts and mammals and suggest a key role for *Osx* in intramembranous and perichondral bone formation in non-mammalian vertebrates such as medaka.

## MATERIALS AND METHODS

### Fish strains, design of *osx* guide RNAs, generation and genotyping of mutants

All wild-type and transgenic medaka strains were described previously (Renn and Winkler, 2009; Renn et al., 2013). Fish were kept at 26°C under a controlled light cycle (14 h light, 10 h dark) to induce spawning. Embryos were kept in 0.3× Danieau's solution [19.3 mM NaCl, 0.23 mM KCl, 0.13 mM MgSO<sub>4</sub>, 0.2 mM Ca(NO<sub>3</sub>)<sub>2</sub>, 1.7 mM HEPES, pH 7.0] at 30°C. All experiments were performed in accordance with approved Institutional Animal Care and Use Committee protocols of the National University of Singapore (R14-293). *osx* gRNAs were designed according to Hwang et al. (2013) and prepared as described in the supplementary Materials and Methods. Purified gRNAs (100 ng/μl each) were co-injected with Cas9 mRNA (300 ng/μl) into medaka embryos at the one-cell stage. Adult potential founders were genotyped by fin clipping and incrossed to obtain germline mosaic F1 embryos. Adult genotyped F1 fish were outcrossed with wild-type fish to obtain heterozygous F2 fish. Homozygous carriers in F3 were analysed for phenotype. For genotyping, larvae or adult fish were anaesthetized with 0.01% or 0.005% ethyl 3-aminobenzoate methanesulfonate (Tricaine; Sigma), respectively. Larvae or clipped caudal fin fragments were lysed individually in 50 μl of 50 mM NaOH and incubated at 95°C for 15 min. Samples were neutralized with 5 μl of 1 M Tris-HCl (pH 8.0). Stained embryos were fixed and washed with 1× phosphate buffered saline with 0.1% (v/v) Tween 20 (PBST) five times before genomic DNA isolation. Larvae were lysed individually with DNA lysis buffer (10 mM Tris-HCl pH 8.2, 50 mM KCl, 0.3% NP 40, 0.3% Tween) and Proteinase K (20 μg/ml; Sigma) with a ratio of 49:1 and incubated at 55°C for 60 min and 90°C for 10 min. The supernatant contained genomic DNA for analysis. A 430 bp fragment was amplified (using primers AACTCGCTATGGCTCCAGT and GAGCCGTAAGGGTGTGTCAT) and digested with *Hae*III (New England Biolabs). Mutants showed undigested fragments that were sequenced (Fig. S3).

### Analysis of *Osx* relationships within vertebrates

Analyses of phylogenetic relationships and synteny conservation were carried out with sequences retrieved from publicly available genome data using previously published bioinformatic tools. For further details, see supplementary Materials and Methods.

### Whole-mount *in situ* hybridization, cartilage and bone staining

*In situ* hybridization and Alcian Blue and Alizarin Red staining were carried out as described (Renn and Winkler, 2009). Microdissection of cartilage was performed according to DeLaurier et al. (2010). Imaging was performed according to To et al. (2012).

### Histological analysis and electron microscopy

Specimens were fixed in a mixture of 1.5% glutaraldehyde/1.5% paraformaldehyde in 0.1 M cacodylate buffer for 24 h prior to decalcification in 10% EDTA for a minimum of 48 h. Specimens were postfixed with osmium tetroxide and embedded in Epon epoxy resin. Semi-

thin sections (1 μm) were stained with Toluidine Blue for 1 min (0.2% Toluidine Blue, 2% Na<sub>2</sub>CO<sub>3</sub>), rinsed with water, air-dried, mounted with DPX (Fluka, Switzerland) and analysed with a Zeiss Axio Imager Z compound microscope. Ultrathin sections (0.02 μm) from the same blocks were contrasted with uranyl acetate and lead citrate and observed with a Jeol JEM 1010 transmission electron microscope operating at 60 kV. Images were digitized using a DITABIS drum scanner.

### Imaging

For live fluorescence imaging, larvae were anaesthetized with 0.01% Tricaine (Sigma) and pictures were taken using a Nikon SMZ1000 stereomicroscope equipped with NIS-Elements BR 3.0 software (Nikon). For live confocal imaging, larvae were anaesthetized with 0.005% Tricaine and embedded in 1.5% low melting agarose in a glass-bottom Petri dish. Confocal pictures were taken with a Zeiss LSM 510 Meta using 488 and 543 nm laser lines for GFP and mCherry analysis, respectively. Whole-mount fixed larvae and samples after microdissection were mounted in 100% glycerol for photography with a Nikon SMZ1000 stereomicroscope and a Nikon Eclipse 90i upright microscope equipped with NIS-Elements BR 3.0 software (Nikon). Imaging data were processed using Zeiss LSM Image Browser Version 4.2.0.121, ImageJ and Adobe Photoshop CS6 software.

### RT-PCR

Twenty larvae at 12 dpf were used for RNA extraction using the RNeasy Mini Kit (QIAGEN). Wild-type larvae served as control. All RNA samples were subjected to DNase I digestion. RNA was reverse transcribed using the RevertAid First Strand cDNA Synthesis Kit (Life Technologies). *β-actin* was used for normalization. The following primers were used: *β-actin* (TTCAA-CAGCCCTGCCATGTA, GCAGCTCATAGCTCTTCTCCAGGGAG); *osx* (TCTCCCCTCAGCTTCCTTAG, CTGGAAAGAGTGGGAGAAGG); *osc* (GAACCCGAGGTTATTGTGGA, TCACAGGCAACGTTTCAGTTC).

### Quantitative real-time PCR (qPCR)

cDNA of *osx* mutants and wild-type controls were used for qPCR. *β-actin* was used for normalization. The following primers were used: *β-actin* (GCCAACAGGGAGAAGATGAC, CATCACCAGAGTCCATGACG); *osx* (CAGATAAGACCGGCAGCAC, TCCTCCAGCTGTGGTGAAG). Comparisons of the gene expression levels in *osx* mutants relative to WT controls were performed in triplicate and analysed using Prism7000 software. A two-tailed Student's *t*-test was performed for statistical analysis.

### Acknowledgements

We thank the members of the confocal unit of the NUS Centre for Bioimaging Sciences (CBIS) for their constant support.

### Competing interests

The authors declare no competing or financial interests.

### Author contributions

Conceptualization: T.Y., J.R., M.S., A.H., P.E.W., C.W.; Methodology: T.Y., M.G., J.R., M.S., D.L., A.H., P.E.W., C.W.; Formal analysis and investigation: T.Y., M.S., D.L., A.H., P.E.W., C.W.; Writing – original draft preparation: T.Y., M.S., C.W.; Writing – review and editing: T.Y., M.G., J.R., M.S., A.H., P.E.W., C.W.; Funding acquisition: C.W.; Resources: T.Y., M.G., J.R., M.S., A.H., P.E.W., C.W.; Supervision: M.S., A.H., P.E.W., C.W.

### Funding

This project is funded by a Tier 2 grant from the Ministry of Education - Singapore (MOE) [2013-T2-2-126]. T.Y. and M.G. received graduate fellowships from the National University of Singapore.

### Supplementary information

Supplementary information available online at <http://dev.biologists.org/lookup/doi/10.1242/dev.139550.supplemental>

### References

Akiyama, H., Kim, J.-E., Nakashima, K., Balmes, G., Iwai, N., Deng, J. M., Zhang, Z., Martin, J. F., Behringer, R. R., Nakamura, T. et al. (2005). Osteochondroprogenitor cells are derived from Sox9 expressing precursors. *Proc. Natl. Acad. Sci. USA* **102**, 14665–14670.

- Baek, W.-Y., de Crombrughe, B. and Kim, J.-E. (2010). Postnatally induced inactivation of Osterix in osteoblasts results in the reduction of bone formation and maintenance. *Bone* **46**, 920–928.
- Bensimon-Brito, A., Cancela, M. L., Huysseune, A. and Witten, P. E. (2012a). Vestiges, rudiments and fusion events: the zebrafish caudal fin endoskeleton in an evo-devo perspective. *Evol. Dev.* **14**, 116–127.
- Bensimon-Brito, A., Cardeira, J., Cancela, M. L., Huysseune, A. and Witten, P. E. (2012b). Distinct patterns of notochord mineralization in zebrafish coincide with the localization of Osteocalcin isoform 1 during early vertebral centra formation. *BMC Dev. Biol.* **12**, 28.
- DeLaurier, A., Eames, B. F., Blanco-Sánchez, B., Peng, G., He, X., Swartz, M. E., Ullmann, B., Westerfield, M. and Kimmel, C. B. (2010). Zebrafish sp7:EGFP: a transgenic for studying otic vesicle formation, skeletogenesis, and bone regeneration. *Genesis* **48**, 505–511.
- Fleming, A., Kishida, M. G., Kimmel, C. B. and Keynes, R. J. (2015). Building the backbone: the development and evolution of vertebral patterning. *Development* **142**, 1733–1744.
- Flores, M. V., Tsang, V. W. K., Hu, W., Kalev-Zylinska, M., Postlethwait, J., Crosier, P., Crosier, K. and Fisher, S. (2004). Duplicate zebrafish runx2 orthologues are expressed in developing skeletal elements. *Gene Expr. Patterns* **4**, 573–581.
- Goto, T., Matsui, Y., Fernandes, R. J., Hanson, D. A., Kubo, T., Yukata, K., Michigami, T., Komori, T., Fujita, T., Yang, L. et al. (2006). Sp1 family of transcription factors regulates the human alpha2 (XI) collagen gene (COL11A2) in Saos-2 osteoblastic cells. *J. Bone Miner. Res.* **21**, 661–673.
- Grothmol, S., Nordvik, K., Kryvi, H. and Totland, G. K. (2005). A segmental pattern of alkaline phosphatase activity within the notochord coincides with the initial formation of the vertebral bodies. *J. Anat.* **206**, 427–436.
- Hammond, C. L. and Schulte-Merker, S. (2009). Two populations of endochondral osteoblasts with differential sensitivity to Hedgehog signalling. *Development* **136**, 3991–4000.
- Harada, S. and Rodan, G. A. (2003). Control of osteoblast function and regulation of bone mass. *Nature* **423**, 349–355.
- Hautier, L., Weisbecker, V., Sanchez-Villagra, M. R., Goswami, A. and Asher, R. J. (2010). Skeletal development in sloths and the evolution of mammalian vertebral patterning. *Proc. Natl. Acad. Sci. USA* **107**, 18903–18908.
- Hojo, H., Ohba, S., He, X., Lai, L. P. and McMahon, A. P. (2016). Sp7/osterix is restricted to bone-forming vertebrates where it acts as a Dlx co-factor in osteoblast specification. *Dev. Cell* **37**, 238–253.
- Huxley, T. H. (1859). Observations on the development of some parts of the skeleton of fishes. *Q. J. Micros. Sci.* **7**, 33–46.
- Hwang, W. Y., Fu, Y., Reyon, D., Maeder, M. L., Tsai, S. Q., Sander, J. D., Peterson, R. T., Yeh, J.-R. J. and Joung, J. K. (2013). Efficient genome editing in zebrafish using a CRISPR-Cas system. *Nat. Biotechnol.* **31**, 227–229.
- Inohaya, K., Takano, Y. and Kudo, A. (2007). The teleost intervertebral region acts as a growth center of the centrum: in vivo visualization of osteoblasts and their progenitors in transgenic fish. *Dev. Dyn.* **236**, 3031–3046.
- Janvier, P. (2015). Facts and fancies about early fossil chordates and vertebrates. *Nature* **520**, 483–489.
- Kague, E., Roy, P., Asselin, G., Hu, G., Simonet, J., Stanley, A., Albertson, C. and Fisher, S. (2016). Osterix/Sp7 limits cranial bone initiation sites and is required for formation of sutures. *Dev. Biol.* **413**, 160–172.
- Kirsch, T. and von der Mark, K. (1992). Remodelling of collagen types I, II and X and calcification of human fetal cartilage. *Bone Miner.* **18**, 107–117.
- Koga, T., Matsui, Y., Asagiri, M., Kodama, T., de Crombrughe, B., Nakashima, K. and Takayanagi, H. (2005). NFAT and Osterix cooperatively regulate bone formation. *Nat. Med.* **11**, 880–885.
- Kölliker, A. (1859). On the structure of the chorda dorsalis of the plagiostomes and some other fishes, and on the relation of its proper sheath to the development of the vertebrae. *Proc. R. Soc. Lond.* **10**, 214–222.
- Lapunzina, P., Aglan, M., Temtamy, S., Caparrós-Martín, J. A., Valencia, M., Letón, R., Martínez-Glez, V., Elhossini, R., Amr, K., Vilaboa, N. et al. (2010). Identification of a frameshift mutation in Osterix in a patient with recessive osteogenesis imperfecta. *Am. J. Hum. Genet.* **87**, 110–114.
- Lauder, G. V. (1980). On the relationship of the myotome to the axial skeleton in vertebrate evolution. *Paleobiology* **6**, 51–56.
- Laue, K., Janicke, M., Plaster, N., Sonntag, C. and Hammerschmidt, M. (2008). Restriction of retinoic acid activity by Cyp26b1 is required for proper timing and patterning of osteogenesis during zebrafish development. *Development* **135**, 3775–3787.
- Li, N., Felber, K., Elks, P., Croucher, P. and Roehl, H. H. (2009). Tracking gene expression during zebrafish osteoblast differentiation. *Dev. Dyn.* **238**, 459–466.
- Long, F. (2012). Building strong bones: molecular regulation of the osteoblast lineage. *Nat. Rev. Mol. Cell Biol.* **13**, 27–38.
- Nakashima, K., Zhou, X., Kunkel, G., Zhang, Z., Deng, J. M., Behringer, R. R. and de Crombrughe, B. (2002). The novel zinc finger-containing transcription factor osterix is required for osteoblast differentiation and bone formation. *Cell* **108**, 17–29.
- Oh, J.-H., Park, S.-Y., de Crombrughe, B. and Kim, J.-E. (2012). Chondrocyte-specific ablation of Osterix leads to impaired endochondral ossification. *Biochem. Biophys. Res. Commun.* **418**, 634–640.
- Renn, J. and Winkler, C. (2009). Osterix-mCherry transgenic medaka for in vivo imaging of bone formation. *Dev. Dyn.* **238**, 241–248.
- Renn, J., Buttner, A., To, T. T., Chan, S. J. and Winkler, C. (2013). A col10a1:nlGFP transgenic line displays putative osteoblast precursors at the medaka notochordal sheath prior to mineralization. *Dev. Biol.* **381**, 134–143.
- Renn, J. and Winkler, C. (2014). Osterix/Sp7 regulates biomineralization of otoliths and bone in medaka (*Oryzias latipes*). *Matrix Biol.* **34**, 193–204.
- Rossi, A., Kontarakis, Z., Gerri, C., Nolte, H., Höpfer, S., Krüger, M. and Stainier, D. Y. R. (2015). Genetic compensation induced by deleterious mutations but not gene knockdowns. *Nature* **524**, 230–233.
- Spoorendonk, K. M., Peterson-Maduro, J., Renn, J., Trowe, T., Kranenbarg, S., Winkler, C. and Schulte-Merker, S. (2008). Retinoic acid and Cyp26b1 are critical regulators of osteogenesis in the axial skeleton. *Development* **135**, 3765–3774.
- To, T. T., Witten, P. E., Renn, J., Bhattacharya, D., Huysseune, A. and Winkler, C. (2012). Rankl-induced osteoclastogenesis leads to loss of mineralization in a medaka osteoporosis model. *Development* **139**, 141–150.
- van Eeden, F. J., Granato, M., Schach, U., Brand, M., Furutani-Seiki, M., Haffter, P., Hammerschmidt, M., Heisenberg, C. P., Jiang, Y. J., Kane, D. A. et al. (1996). Mutations affecting somite formation and patterning in the zebrafish, *Danio rerio*. *Development* **123**, 153–164.
- Witten, P. E., Obach, A., Huysseune, A. and Baeverfjord, G. (2006). Vertebrae fusion in Atlantic salmon (*Salmo salar*): Development, aggravation and pathways of containment. *Aquaculture* **258**, 164–172.
- Witten, P. E. and Huysseune, A. (2009). A comparative view on mechanisms and functions of skeletal remodelling in teleost fish, with special emphasis on osteoclasts and their function. *Biol. Rev. Camb. Philos. Soc.* **84**, 315–346.
- Xu, P., Zhang, X., Wang, X., Li, J., Liu, G., Kuang, Y., Xu, J., Zheng, X., Ren, L., Wang, G. et al. (2014). Genome sequence and genetic diversity of the common carp, *Cyprinus carpio*. *Nat. Genet.* **46**, 1212–1219.
- Ytteborg, E., Todorovic, M., Krasnov, A., Takle, H., Kristiansen, I. O. and Ruyter, B. (2015). Precursor cells from Atlantic salmon (*Salmo salar*) visceral fat holds the plasticity to differentiate into the osteogenic lineage. *Biol. Open* **4**, 783–791.
- Zhang, H., Jiang, Y., Qin, C., Liu, Y., Ho, S. P. and Feng, J. Q. (2015). Essential role of osterix for tooth root but not crown dentin formation. *J. Bone Miner. Res.* **30**, 742–746.
- Zhong, Z., Niu, P., Wang, M., Huang, G., Xu, S., Sun, Y., Xu, X., Hou, Y., Sun, X., Yan, Y. et al. (2016). Targeted disruption of sp7 and myostatin with CRISPR-Cas9 results in severe bone defects and more muscular cells in common carp. *Sci. Rep.* **6**, 22953.
- Zhou, X., Zhang, Z., Feng, J. Q., Dusevich, V. M., Sinha, K., Zhang, H., Darnay, B. G. and de Crombrughe, B. (2010). Multiple functions of Osterix are required for bone growth and homeostasis in postnatal mice. *Proc. Natl. Acad. Sci. USA* **107**, 12919–12924.